C-terminal domain of T4 gene 32 protein enables rapid filament reorganization and dissociation

Ben A. Cashen[1], Michael Morse[1], Ioulia Rouzina[2], Richard L. Karpel[3], Mark C. Williams[1†]

[1]Department of Physics, Northeastern University, 110 Forsyth Street, Boston, MA 02115, USA

[2]Department of Chemistry and Biochemistry, Center for Retroviral Research and Center for RNA Biology, Ohio State University, 281 W Lane Avenue, Columbus, OH 43210, USA

[3]Department of Chemistry and Biochemistry, University of Maryland Baltimore County, 1000 Hilltop Circle, Baltimore, MD 21250, USA

[†]Corresponding author: Tel: +1 617 373 5705; Email: ma.williams@northeastern.edu; Mailing address: 360 Huntington Avenue, Boston, MA 02115, USA

Abstract

Bacteriophage T4 gene 32 protein (gp32) is a single-stranded DNA (ssDNA) binding protein essential for DNA replication. gp32 forms stable protein filaments on ssDNA through cooperative interactions between its core and N-terminal domain. gp32's C-terminal domain (CTD) is believed to primarily help coordinate DNA replication via direct interactions with constituents of the replisome. However, the exact mechanisms of these interactions are not known, and it is unclear how tightly-bound gp32 filaments are readily displaced from ssDNA as required for genomic processing. Here, we utilized truncated gp32 variants to demonstrate a key role of the CTD in regulating gp32 dissociation. Using optical tweezers, we probed the binding and dissociation dynamics of CTD-truncated gp32, *I, to an 8.1 knt ssDNA molecule and compared these measurements with those for full-length gp32. The *I-ssDNA helical filament becomes progressively unwound with increased protein concentration but remains significantly more stable than that of full-length, wild-type gp32. Protein oversaturation, concomitant with filament unwinding, facilitates rapid dissociation of full-length gp32 from across the entire ssDNA segment. In contrast, *I primarily unbinds slowly from only the ends of the cooperative clusters, regardless of the protein density and degree of DNA unwinding. Our results suggest that the CTD may constrain the relative twist angle of proteins within the ssDNA filament such that upon critical unwinding the cooperative interprotein interactions largely vanish, facilitating prompt removal of gp32. We propose a model of CTD-mediated gp32 displacement via internal restructuring of its filament, providing a mechanism for rapid ssDNA clearing during genomic processing.

Keywords

single-stranded DNA binding protein; single molecule; DNA replication; optical tweezers; cooperative protein filament

Abbreviations

gp32, T4 gene 32 protein; ssDNA, single-stranded DNA; dsDNA, double-stranded DNA; FJC, freely jointed chain; WLC, worm-like chain

1. Introduction

T4 bacteriophage is a useful model system for understanding DNA replication [1]. Its replisome closely resembles those of more complex organisms, comprising eight proteins that make up the three major subassemblies characteristic of all higher order systems [1-5]. Gene 32 protein (gp32), the prototypical single-stranded DNA (ssDNA) binding protein, is a key component of the T4 replication, recombination, and repair machinery [6]. Its high affinity, sequence-nonspecific ssDNA binding enables efficient coating of single-stranded regions transiently formed during DNA replication, offering protection from enzymatic degradation. Moreover, gp32's ability to effectively discriminate against duplexed double-stranded DNA (dsDNA) [7, 8] enhances replisome processivity by disrupting the formation of DNA secondary structures that would otherwise inhibit polymerase functionality [9].

The gp32 monomer consists of three distinct domains (see Fig. 1A), each essential for its function during replication: a positively-charged N-terminal domain (NTD, residues 1-21), a central ssDNA binding core (residues 22-253), and a negatively-charged C-terminal domain (CTD, residues 254-301) [10]. The gp32 core domain binds ssDNA in a relatively small, positively-charged cleft (groove), conferring the protein with (largely) sequence-independent, preferential ssDNA binding [7, 8, 11]. Subsequent to initial binding (nucleation), gp32 forms highly stable, cooperative protein filaments along ssDNA, mediated by interactions between the NTD of a nucleic acid-bound monomer and the core domain of an adjacently-bound protein [12, 13]. These flexible protein filaments helically wind the DNA substrate, resulting in simultaneous rigidification and compaction of the ssDNA, characterized by its increased persistence length and reduced contour length, respectively [14-19].

While gp32's highly cooperative nature allows it to form tightly-bound filaments that efficiently protect ssDNA from nuclease attack, such stable binding would seemingly prevent the protein from being easily displaced as required for genomic processing [20, 21]. However, our previous work [14] revealed a mechanism that allows for the rapid recycling of bound protein necessary for prompt DNA synthesis. The helically compacting gp32-ssDNA structures are highly dynamic and possess the ability to interconvert between different wound states as a function of protein density on the DNA. Increased protein density results in progressive unwinding of the helical protein filaments accompanied by significant destabilization and weakening of the cooperative protein-protein contacts. Our results suggested a plausible model for rapid gp32 displacement during DNA replication via its overcrowding on the ssDNA template. However, it is unclear how, or if, the acidic CTD plays a role in this dissociation process.

gp32's C-terminal domain has been shown to modulate gp32-ssDNA interactions via fluctuations between an 'open' and 'closed' state [22]. At low to moderate salt (≤ 200 mM NaCl) the negatively-charged CTD competes with the DNA substrate for access to the protein's cationic binding groove, resulting in reduced overall affinity for ssDNA [22-24]. These competing interactions for the gp32 core domain have been mapped to gp32's atypical salt dependence as well as the 'kinetic block' to dsDNA melting by full-length gp32 observed in thermal melting experiments [22-27]. Removal of the CTD through limited tryptic digestion results in a gp32 truncate, *I, which binds ssDNA cooperatively with increased inherent affinity and exhibits a greater capacity to disrupt and unwind duplexed DNA [24, 28].

In addition to regulating its ssDNA binding and helix-destabilization activities, gp32's CTD has been shown to associate with several replisomal proteins, such as the DNA polymerase, helicase, and helicase loader. [6, 29-32]. These heterotypic protein interactions are believed to primarily help coordinate T4 DNA replication and recombination by stabilizing the binding of the various replisomal proteins to the DNA, thereby facilitating proper assembly of the replication complex [29, 32, 33]. Conversely, T4

replication also requires the efficient removal and subsequent recycling of gp32 from the ssDNA template. Measurements of gp32 displacement by the UvsW and gp41 T4 helicases showed enhanced displacement activity in the presence of the C-terminal domain, and this activity was correlated with CTD-helicase binding, suggesting a role of the acidic CTD in regulating removal of gp32 during genomic processing [34]. However, the exact mechanism of interaction is not known, and it is unclear how protein-protein binding can enable the fast displacement of gp32 necessary for rapid strand synthesis.

To investigate the role of the CTD in regulating gp32 removal, we probed the binding and dissociation dynamics of C-terminal truncates, *I and *III (Fig. 1A), with a long (8.1 knt) ssDNA substrate and compared these measurements with the CTD-intact, full-length and *II proteins. Our most recent study [14] revealed dynamic gp32-ssDNA filament unwinding in response to increased protein density along the DNA. Moreover, a critical level of unwinding gave rise to an unstable protein state, resulting in fast, noncooperative gp32 dissociation from across the entire ssDNA segment, suggesting a plausible mode of rapid template clearing during movement of the replication fork. Here, we extend this work and show that the CTD plays an essential role in facilitating this prompt filament reorganization and dissociation. Upon removal of the CTD, the fast, noncooperative gp32 dissociation phase vanishes and the ssDNA-bound protein cluster remains highly stable and cooperative, with its protein components released slowly, only from the ends of the filament, regardless of the protein density and degree of DNA unwinding. Unlike intact gp32, the rate of ssDNA release from the protein filament is significantly slower than the rate of T4 DNA synthesis.

2. Results and Discussion

Using optical tweezers, we observed the binding of the C-terminal (CTD) truncated gp32 variant, *I (Fig. 1A), to an 8.1 knt ssDNA molecule by measuring the extension of the protein-DNA complex held under constant tension (Fig. 1B-C). Additionally, we compared these measurements with those previously taken with wild-type (WT) gp32 [14] in order to quantify the extent to which gp32-ssDNA interactions are modulated by the protein's CTD. Similar to WT gp32 (Fig. 1C, light blue), during incubation with *I (blue) we observe up to three sequential steps of DNA compaction and elongation ($\Delta x_+^{1\text{-}3}$) before the protein-DNA complex equilibrates to a final extension. However, the binding profile of *I exhibits significantly less compaction than that of WT gp32, attaining a more elongated conformation at equilibrium. When free protein is replaced with protein-free buffer, initial dissociation results in similar (linear over time) substrate recompaction (Δx_-^1) for both the WT gp32 (light red) and *I (red) complexes.

We previously interpreted these multiphasic length changes in terms of winding and unwinding of the DNA by gp32 [14]. Our prior work suggested that gp32 filaments helically wind the ssDNA [15-19], resulting in significant substrate compaction (Δx_+^1) upon initial protein binding and filamentation. Following compaction, additional gp32 binding into the saturated complex resulted in elongation of the DNA ($\Delta x_+^1 \rightarrow \Delta x_+^2$ and $\Delta x_+^2 \rightarrow \Delta x_+^3$) to a less compact equilibrium state, likely reflecting partial unwinding of the helical protein structures. Furthermore, upon removal of free protein (initial dissociation), the elongation was reversed (recompaction, Δx_-^1) as the extension of the complex returned to its original compacted length, indicating rewinding of the released ssDNA on the remaining gp32 filaments.

Here, we interpret our *I binding data within the same framework used to model the previously observed WT gp32 dynamics. Thus, differences in the binding and dissociation profiles of WT gp32 and *I

can be used to assess the impact of the CTD on gp32's ability to dynamically wind and unwind the DNA in response to various solution conditions. For example, the significantly less compact *I-ssDNA equilibrium state (Fig. 1C) suggests that at equivalent protein concentrations, the *I complex is considerably less wound (i.e., has greater helical pitch) than WT gp32. However, the similarity in dissociation profiles indicates that under these conditions both proteins unbind from and rewind the ssDNA in a similar fashion. We analyze in detail how this behavior varies with respect to protein and salt (Na^+) concentration by measuring the amplitudes and rates associated with each distinct step of DNA compaction and elongation.

2.1. Binding dynamics of noncooperative *II and *III truncates

We first probed the effect of the CTD in the absence of cooperative interactions (i.e., protein filamentation) by comparing the binding and dissociation profiles of the noncooperative gp32 truncates, *II and *III, which lack the N-terminal domain (NTD) required for homotypic protein interactions (see Fig. 1A). As shown previously [14], in the absence of the NTD, gp32 is unable to form cooperative protein filaments that helically wind the ssDNA, resulting in single-phased binding and dissociation profiles with significantly reduced compaction. We observe nearly identical substrate compaction at protein saturation (Fig. 2A-C), well fit by a single observed rate constant (k_{obs}), for gp32 with (*II) and without (*III) the CTD. However, the concentration of protein required to saturate the ssDNA is greatly reduced upon removal of the CTD, and the measured rates of binding and dissociation are markedly different. Assuming the rate of equilibration observed during incubation is the sum of the concentration-dependent rate of protein association and the (constant) rate of protein dissociation ($k_{obs} = ck_{on} + k_{off}$), we compute the fundamental concentration-independent rate of free protein binding (Fig. 2D-E). The calculated bimolecular on-rate of *III (0.064±0.007 $nM^{-1}s^{-1}$) is ~25-fold higher than that of *II, while the off-rate (0.064±0.006 s^{-1}) is ~2-fold lower. By comparison, prior ensemble measurements of gp32 binding [35] showed a similar ~20-fold increase in noncooperative protein association (k_{on}) upon removal of the CTD (50 mM NaCl). Thus, the negatively-charged C-terminal domain lowers gp32-ssDNA binding affinity by over an order of magnitude ($K_D^{*II}/K_D^{*III} \approx 50$), consistent with previous studies [22, 25-27] showing that at moderate and low salt (≤ 200 mM NaCl) the acidic CTD can compete with the DNA substrate, adopting a 'closed' conformation in which it partially (or totally) occludes the protein's ssDNA binding site. Our results imply that these competing interactions of the C-terminal domain with the gp32 core domain drastically reduce the rate of protein association with the DNA substrate (Fig. 2F), while moderately facilitating ssDNA release (dissociation) from the protein's cationic binding groove (Fig. 2G), resulting in an overall ~50-fold reduction in gp32 binding affinity at 15 pN.

We also compared the force response of the noncooperative protein complexes by slowly stretching the DNA in the presence of saturating (1 μM) concentrations of *II and *III. The DNA was extended at a rate of ~10 nm/s, such that the tension along the substrate increased from 0 to 70 pN over the course of ~5 min, to ensure equilibration of the gp32-ssDNA complexes during stretching. The resulting force-extension curves (FECs) show similar behavior between the two proteins (Fig. S1A-B); the DNA is measurably shortened at high force (> 10 pN) and extended at low force (< 10 pN) due to changes in its contour and persistence lengths, respectively. We fit the FEC of the *III-saturated DNA with the freely jointed chain (FJC, see Materials and Methods) polymer model [36] up to 10 pN to compute an average contour length of 0.52±0.01 nm/nt and a persistence length of 2.2±0.2 nm, comparable to the values measured previously for *II (Fig. S1C-D). Consistent with the binding at 15 pN (Fig. 2), these results indicate that, while the CTD modulates the rates of gp32 binding and dissociation, in the absence of

cooperativity it does not significantly alter the equilibrium conformation of the saturated protein-DNA complex.

2.2. Concentration dependence of *I binding

We probed the concentration dependence of *I binding to ssDNA held at 15 pN tension by measuring the extension change of the DNA as a function of various saturating protein concentrations. In contrast to the single-phased binding profiles of the noncooperative gp32 truncates, *I exhibits multiphasic binding (Fig. 3A-C) associated with winding (compaction) and unwinding (elongation) of the DNA by the cooperative protein filaments as previously observed with WT gp32. Both the transient compaction (Δx_+^1) and equilibrium compaction (Δx_+^3) of the DNA decrease with *I concentration, indicative of increased DNA unwinding. Rapid elongation ($\Delta x_+^1 \rightarrow \Delta x_+^2$) subsequent to the initial compaction step is only observed at [*I] ≥ 10 nM but continues to grow in amplitude as protein concentration is increased. Additionally, the slow, secondary elongation step ($\Delta x_+^2 \rightarrow \Delta x_+^3$) vanishes when [*I] is reduced to 0.5 nM as the binding profile becomes single-phased and the protein-DNA complex equilibrates to a highly compact (wound) state. Overall, this behavior qualitatively mimics that observed previously with WT gp32 [14], suggesting similar modes of protein binding (i.e., rapid DNA winding followed by partial unwinding, concomitant with additional binding into the saturated complex). In general, however, the *I complex is considerably more elongated at equilibrium relative to WT gp32, indicating that removal of gp32's C-terminal domain facilitates transition to a less-wound protein-DNA conformation.

The binding kinetics were evaluated by measuring the transition rates associated with each distinct step of DNA compaction and elongation (Fig. 3D-G). Similar to WT gp32, the rate of DNA compaction (k_+^1) initially increases linearly with *I concentration before reaching an asymptote at high protein concentrations. However, this rate is shifted to (~20-fold) lower concentrations relative to WT, consistent with an increase in ssDNA binding affinity (i.e., faster protein association) upon removal of the CTD, as observed with *III (Fig. 2). Formation of the compacting gp32-ssDNA filaments ($\Delta x_0 \rightarrow \Delta x_+^1$) is a multistep process involving: (i) protein nucleation events (i.e., initial binding and formation of noncooperatively-bound gp32), followed by (ii) initial cluster formation and filament growth along the DNA [14, 37]. At low bulk gp32 concentrations, k_+^1 is linear in [gp32], indicating rate-limiting by the bimolecular association of free protein with the DNA substrate (i.e., slow binding regime). However, at very high concentrations (i.e., fast binding regime), the rate of compaction becomes dominated by the kinetics of filament formation and subsequent DNA winding. We, therefore, fit k_+^1 with a two-step reaction model allowing us to decouple the protein's bimolecular binding, k_b, from the rate of subsequent compaction, k_c, due to initial cluster formation (oligomerization), as described previously [14]. We measure a *I on-rate (defined by the slope of the linear k_+^1 vs [gp32] region, Fig. 3D-E) of 0.056±0.006 $nM^{-1}s^{-1}$, ~20-fold higher than that of WT gp32, in good agreement with the calculated on-rate of *III (Fig. 2D), and consistent with previously reported measurements of gp32 binding from stopped-flow experiments [35]. In contrast, the asymptote of k_+^1, which defines the rate of *I oligomerization (k_c = 1.3±0.2 s^{-1}, Fig. 3D, F), is comparable to that of the full-length protein. Taken together, these results suggest that, while the CTD presents a barrier to initial gp32-DNA association (i.e., competes with the ssDNA for access to the protein's binding site), it does not significantly alter the timescale of subsequent filament formation along the DNA substrate.

The rapid elongation phase occurring at [*I] ≥ 10 nM (k_+^2, Fig. 3D) is marginally slower than the initial DNA compaction step but exhibits a comparable rate increase with protein concentration, suggesting

that this phase of elongation may reflect a similar process of protein binding. In contrast, the slow secondary elongation phase (k_+^3) is independent of free protein concentration, indicating an additional rate-limiting step to the restructuring of the protein-DNA complex, consistent with the behavior observed previously for WT gp32. Notably, however, this transition is ~2-fold slower than that of the full-length protein (Fig. 3G). As this phase of DNA elongation is likely driven by additional binding into the saturated complex [14], we previously hypothesized that its transition rate may reflect a timescale of breaking gp32-gp32 contacts in order to accommodate additional protein into the existing cooperative filament. However, this process must also involve partial unwinding of the DNA, concomitant with its peeling (partial release) from the protein's binding groove in pre-equilibrium to the binding of additional gp32 into the saturated filament. As seen with the noncooperative truncates, *II and *III, ssDNA release from the gp32 core domain is facilitated by competing interactions of the CTD with the protein's binding site (Fig. 2G). Thus, while this phase of slow (~100 s) filament restructuring may be dominated by the rate of protein-protein uncoupling (i.e., depolymerization), the moderate increase in k_+^3 observed for WT gp32 could primarily be a consequence of CTD-mediated changes in the protein's core-ssDNA interaction, allowing the protein-DNA filament to reorganize on shorter timescales.

2.3. Polymer and helical parameters of the *I-ssDNA complex

To further probe the effects of the CTD on the structural details of the gp32-ssDNA complex, we slowly stretched the DNA (~10 nm/s to maintain equilibrium) in the presence of different concentrations of *I and compared these measurements with those previously taken with WT gp32. In contrast to the noncooperative truncates, *II and *III, the strong interprotein interactions of *I and WT gp32 allow the protein to form long, continuous filaments that helically wind the DNA, resulting in additional substrate compaction at high force (≥ 10 pN) and elongation at low force (≤ 10 pN) due to changes in the DNA contour and persistence lengths, respectively. Similar to WT gp32, the ssDNA becomes significantly more extended with increased *I concentration (Fig. 4A), consistent with the elongation observed during constant force measurements (Fig. 3A-B). We fit the *I force-extension curves with the worm-like chain (WLC, see Materials and Methods) model [38, 39] up to 5 pN (inset) to compute the average contour and persistence lengths of the *I-ssDNA complex as functions of free protein concentration (Fig. 4B-C). The *I complexes exhibit significantly (~10-fold) greater persistence lengths than the noncooperative protein-DNA complexes, reflecting rigidification of the ssDNA upon protein filamentation. Additionally, the *I-ssDNA persistence length remains constant across the range of saturating concentrations studied and corresponds with that of the WT gp32 complex (~20 nm) at high concentration (≥ 25 nM), in reasonable agreement with previous light scattering experiments [40]. In contrast, the ssDNA contour length gradually increases with *I concentration relative to its compacted state. Thus, similar to full-length gp32, increased elongation of the *I complex with concentration is primarily driven by an increase in the contour length of the DNA, associated with filament unwinding. However, at similar bulk protein concentrations, *I exhibits a significantly smaller contour length reduction (i.e., is more extended) than WT gp32, indicating greater unwinding of the *I-ssDNA filament at equilibrium.

We modeled the *I complex as an ideal protein-DNA helix in which the DNA is continuously wrapped around the gp32 filament, allowing us to map the measured contour length changes (Fig. 4C) to different wound states of the protein complex [14]. The geometrical parameters of an ideal protein-DNA helical filament are related as follows:

$$\frac{R}{\rho} = \frac{1}{2\pi}\left[\left(\frac{L}{L'}\right)^2 - 1\right]^{1/2} \quad (1)$$

where R is the helix radius, ρ is the helical pitch (length per turn), L is the contour length of bare ssDNA per nt (0.56 nm/nt), and L' is the effective contour length of the protein-DNA complex per nt (length along the translational axis, see Fig. 4D). Assuming an ideal helical structure with a constant filament radius of ~2 nm, as measured previously for WT gp32 [14, 15], we calculate a *I-ssDNA helical pitch of 14.2±0.7 nm (or ρ/L' = 35±2 nt of wound ssDNA per turn) at the lowest saturating bulk protein concentration of 0.5 nM, corresponding to its most compact, wound state (L' = 0.41±0.01 nm/nt, see Fig. 3A). Assuming that in this most relaxed and optimally wound filament state the gp32 binding site size on ssDNA is 7 nt, as measured previously [10], we estimate the length of ssDNA per protein along the helical axis, h = 0.41 nm/nt · 7 nt = 2.9±0.1 nm, as well as the number of proteins per helical turn, N = 35 nt/7 nt = 5±0.3, consistent with the values found previously for WT gp32 [14].

As we titrated in additional *I, the equilibrium complex extension became more elongated (Fig. 4A), corresponding to a continual increase in the helical pitch of the gp32 filament according to Eq. (1) (Fig. 4E). Assuming the length, h, of each *I protein along the filament axis remains constant, the observed filament lengthening implies that more proteins join the filament and the protein binding site size (*bss*) on ssDNA shrinks according to the expression $bss = h/L'$ (Fig. 4G). Furthermore, as additional gp32 bind into the complex, the number of proteins bound per turn, $N = \rho/h$ grows (Fig. S2), while the twist angle between neighboring proteins, $\alpha = 360°/N$ decreases (Fig. 4F). Both protein filaments reveal highly dynamic structures, with the ability to adopt multiple wound states, in good agreement with the multiphasic binding observed during constant force measurements (Fig. 3A-C). However, the changes in the helical parameters are significantly greater for the *I complex, consistent with greater unwinding of the DNA substrate with concentration.

2.4. Concentration dependence of *I dissociation

To measure the effects of the CTD on gp32 dissociation, we first initialized the complex in different wound states by incubating the DNA with various concentrations of *I. Upon removal of free protein, initial dissociation of *I results in substrate recompaction (Δx^{-1}), associated with rewinding of the released ssDNA on the remaining gp32 filament (Fig. 5A). Recompaction of the protein-DNA complex is linear in time (rather than exponential), indicating dissociation of *I primarily from the ends of the cooperative protein filaments [20, 21, 41]. Notably, recompaction of the *I complex remains linear across all incubation concentrations studied. That is, regardless of the protein density (Fig. 4G) and degree of DNA unwinding, *I unbinds from only the ends of the cooperative clusters. This dissociation profile is comparable to the dissociation of WT gp32 at lower complex saturation [14]. However, at high concentrations of full-length gp32 (≥ 300 nM) we observed the appearance of an initial rapid recompaction step, occurring exponentially over time (Fig. 5B). These previous data suggested a critical level of filament unwinding (dashed line in Fig. 4G), above which the cooperative interactions largely vanish, resulting in rapid gp32 dissociation from across the entire ssDNA segment. This fast (exponential) dissociation continues until the torsional stress of the excess proteins is relieved below its critical value, at which point the protein filament becomes stable, leading to slower (linear) gp32 unbinding only from its ends. This concentration-dependent response is not observed with *I, however, suggesting that the

protein-DNA filament remains stable and cooperative even under conditions in which it is highly oversaturated and unwound. Thus, in the absence of the CTD the gp32-gp32 contacts may be significantly more flexible, allowing the DNA substrate to extend and unwind without dramatically weakening their interprotein stacking interaction.

In order to compare directly the rates of WT and *I dissociation, we calculated a DNA recompaction rate by isolating the portion of each curve spanning the onset of compaction to the completion of half the total extension change exhibited over the entire experiment. This half-compaction data fully includes the fast exponential component of the curve when present, and we define the average rate of compaction over this timescale as $k_{1/2}$. At incubation concentrations ≤ 100 nM, DNA recompaction is linear for both WT gp32 and *I, and the estimated dissociation rate is comparable for the two proteins (Fig. 5C), suggesting that at lower complex saturation both proteins unbind and rewind the DNA in a similar manner. At higher concentrations (≥ 300 nM), however, the rate of WT recompaction increases significantly as dissociation becomes noncooperative, sharply diverging from that of the *I complex, which remains relatively slow and linear. Thus, unlike full-length gp32, upon substrate overcrowding and filament unwinding, dissociation of protein from the *I-DNA complex continues to result solely from slow unbinding at the ends of the protein clusters.

2.5. Salt dependence of *I and WT gp32 binding and dissociation

In lower salt buffers (e.g., 50 mM Na^+) the negatively-charged CTD lowers gp32-ssDNA affinity by associating with the positively-charged surface at or near the protein's cationic binding site, thus competing with ssDNA and resulting in faster protein dissociation as observed with the noncooperative gp32 truncates (Fig. 2G). However, high salt (≥ 200 mM Na^+) effectively screens this interaction, inhibiting formation of the CTD-closed protein state, as modeled previously [22]. Thus, to test if the differences in the WT and *I dissociation profiles are due to competing interactions of the CTD, we measured gp32 binding and dissociation, with and without the CTD, as a function of salt (Na^+) concentration. Both the *I and WT gp32 complexes exhibit increased substrate compaction with increased Na^+ concentration during binding (Fig. 6A), indicating reduced unwinding of the protein-DNA filaments at equilibrium (i.e., lower ssDNA oversaturation). However, the binding profile of *I shows a greater sensitivity to salt, converging with that of WT gp32 at 300 mM Na^+, despite exhibiting greatly reduced compaction (unwinding) at lower [Na^+].

Prior kinetic measurements reported an increase in the bimolecular association rate of gp32 with increased [NaCl], consistent with the highly salt-dependent opening of the acidic CTD near the protein's binding site [35, 37]. However, above ~200 mM NaCl, the rate of protein association decreased, implying weaker electrostatic interactions between ssDNA and the gp32 core domain. By comparison, our binding measurements reveal monotonically decreasing rates of initial compaction (k_+^1) and subsequent fast elongation (k_+^2) of the DNA with increased salt (Fig. 6B), which become more pronounced in the absence of the negatively-charged CTD. At such high bulk protein concentrations (1 μM), these binding phases are presumably rate-dominated by the timescale of gp32 filament formation and ssDNA winding/unwinding rather than the rapid bimolecular association of free protein with the DNA substrate (Fig. 3D). Thus, salt-dependent changes in the bimolecular binding rate, as observed in previous studies, may not contribute significantly to the measured rates of DNA compaction and elongation seen here. Taken together, these results suggest that increases in salt concentration may (slightly) lower the rate of gp32-ssDNA filament formation along the DNA, resulting in moderately reduced rates of DNA winding.

Furthermore, the kinetics of the corresponding *I and WT gp32 binding phases (k_+^1 and k_+^2) converge at high salt, indicating similar rates of filament formation and ssDNA association for both proteins, in reasonable agreement with stopped-flow measurements [35]. This behavior also implies nearly complete screening of the CTD from the protein's binding groove, consistent with the calculated probability of CTD opening, $P_{op} \approx 0.85$ at 300 mM Na^+, as modeled previously [22]. In contrast, the rate of the slow secondary elongation phase (k_+^3) increases ~3 to 4-fold with [Na^+] for both proteins (Fig. 6C). As salt lowers gp32 binding affinity (i.e., increases the rate of protein dissociation, see Fig. S3), the observed increase in k_+^3 is consistent with the hypothesis that slow (~10-100 s) reorganization of the protein-DNA complex is rate-limited by protein unbinding events. That is, salt-induced gp32 destabilization may facilitate partial release of the ssDNA from the protein's core as well as breaking of the cooperative gp32-gp32 contacts in order to accommodate additional protein into the saturated complex, allowing the filament to reorganize on shorter timescales. Notably, this elongation phase remains slightly slower for *I at high salt, suggesting that even a relatively low probability of CTD closing ($P_{cl} \approx 0.15$) may have a measurable impact on the rate of gp32 unbinding and subsequent filament restructuring.

Upon removal of free protein, the dissociation profile of *I remains linear with increased salt, while WT gp32 exhibits biphasic recompaction characteristic of critical filament unwinding (Fig. 6D). The linearity of *I recompaction, preserved across salt conditions, implies that protein binding remains moderately cooperative, such that dissociation occurs primarily from the filament ends. In contrast, the WT gp32 complex exhibits rapid, noncooperative recompaction that persists even at high [Na^+]. As the CTD predominately exists in an 'open' conformation (i.e., does not occlude the ssDNA binding groove) at high salt, this behavior suggests that fast, exponential gp32 dissociation is not primarily due to competing interactions of the CTD with the protein's binding site. Rather, the CTD may interfere with the gp32-gp32 contacts such that critical filament unwinding disrupts the cooperative interprotein interactions, facilitating prompt removal of gp32 from anywhere along the overcrowded ssDNA.

The DNA recompaction rate, $k_{1/2}$ (Fig. 6E), increases with [Na^+] for both *I and WT gp32, indicating faster protein unbinding and weaker electrostatics. The estimated rate of *I recompaction remains ~3-fold slower than that of the full-length protein, primarily due to its lack of exponential (noncooperative) dissociation upon filament unwinding (Fig. 6D, S3). However, the linear recompaction rate is comparable for the two proteins (Fig. S3A), suggesting that the salt dependence of this dissociation phase (i.e., unbinding from the filament ends) is dominated by the salt dependence of gp32-gp32 interactions that are largely insensitive to the presence of the CTD at lower saturation levels.

We also probed the final dissociation phase of *I and WT gp32 at 300 mM Na^+ (Fig. 6F). Once the maximum ssDNA winding within the filament is achieved (Δx_-^1), subsequent (final) gp32 dissociation leads to ssDNA release from the filament followed by an increase in the extension of the complex. While both proteins dissociate fully, returning the complex to its original extension prior to incubation ($\Delta x = 0$), final dissociation of WT gp32 is slightly faster than *I (Fig. 6F inset), suggesting minor destabilization of the gp32 core-ssDNA interaction in the presence of the CTD in high salt. In contrast to the drastically different rates of WT and *I recompaction (initial dissociation, $k_{1/2}$), these data imply that, upon optimal winding (i.e., maximum compaction) of the protein-DNA filament, the *I complex is only moderately more stable than full-length gp32. However, the differences in protein stability become considerably more pronounced, with *I remaining stable and WT gp32 becoming increasingly labile, under conditions in which the structures are highly unwound and elongated. This suggests that the interprotein contacts

of gp32 are significantly more flexible (i.e., proteins can twist freely around the filament axis with minimal disruption) upon removal of the CTD, enabling progressive filament unwinding without significant loss of protein cooperativity.

Rapid WT dissociation, concomitant with critical filament unwinding, occurs over a wide range of NaCl concentrations. However, it is important to note that Cl^- is not the major monovalent anion in the cell, and thus the solution conditions used here are not perfectly representative of those found *in vivo*. Potassium glutamate (KGlu), the primary monovalent salt in bacteria [42, 43], was shown to enhance non-nearest-neighbor cooperativity of the *E. coli* ssDNA binding protein (*Ec*SSB), a property inhibited by KCl [44, 45]. Similar to *Ec*SSB, gp32 binding is sensitive to the type of anion as well as its concentration [22, 46], suggesting possible salt type effects on gp32-ssDNA and gp32-gp32 interactions that are not captured by our binding measurements. Thus, additional studies are required to fully understand the effects of salt type on the filament dynamics seen here.

2.6. Role of gp32's CTD during DNA replication and recombination

In addition to regulating the protein's ssDNA binding and DNA helix-destabilization activities, gp32's C-terminal domain is believed to primarily help coordinate T4 DNA replication and recombination via structural and/or functional interactions with constituents of the replisome machinery. gp32 has been shown to associate with several replisomal proteins, such as the polymerase (gp43), helicase loader (gp59), and the primase (gp61), and these interactions are all abolished by removal of the acidic CTD [47, 48]. Measurements of primase synthesis and processivity showed drastically reduced primer synthesis and faster primase dissociation (resulting in abnormally long and broadly distributed Okazaki fragments) in the absence of the CTD, suggesting a role in stabilizing primase binding to the helicase within the replisome [32]. Similarly, CTD-meditated species-specific interactions between gp32 and T4 DNA polymerase are thought to stabilize binding of the polymerase at the replication fork, thereby stimulating *in vitro* DNA synthesis rates and replisome processivity [47, 49].

On the other hand, rapid displacement of gp32 from transient stretches of ssDNA is also critical for replisome functionality. gp32 must be quickly removed during genomic processing to ensure fast protein recycling, and to clear the way for proper assembly and functioning of various replication and recombination proteins, such as the polymerase, helicase (gp41), and recombinase (UvsX). Measurements of gp32 displacement by the UvsW and gp41 helicases showed increased protein displacement activity in the presence of the CTD, and these data were correlated with CTD-helicase binding [34]. Additionally, direct interactions of gp32 with the helicase loader, gp59, are thought to destabilize or displace gp32 from the ssDNA, exposing a binding site for the helicase [50-52]. The negatively-charged C-terminal domain is clearly essential in regulating the removal of gp32 from ssDNA. However, the molecular mechanism that drives gp32 displacement and prompt ssDNA clearing via direct interactions with its CTD is not understood. How the CTD facilitates rapid removal and recycling of tightly-bound gp32 filaments from long stretches of ssDNA during movement of the replication fork remains an important, open question.

2.6.1 Lagging strand synthesis

Here, we offer an alternative role of the CTD in mediating gp32 removal from ssDNA. Specifically, our experiments show a mode of rapid, noncooperative dissociation of excess gp32 from ssDNA that is not observed in the absence of the CTD. gp32 forms highly cooperative, compacting filaments on the ssDNA

template by stacking into a helix, with each subsequent protein twisted around the filament axis by a definite angle with respect to the previous one [15-19]. The ssDNA binding groove on the gp32 core domain is likely located on the outside of the protein filament, allowing the complex to form a continuous helical path for the ssDNA. Therefore, the twist angle between contiguously-bound gp32 proteins defines the helical pitch of the filament, the overall DNA shortening (i.e., contour length reduction), and the protein density on the ssDNA template. Interestingly, all of the above parameters of the gp32-ssDNA filament can vary widely, leading, in particular, to the occluded binding site size of each protein shrinking from ~7 to ~5 nt with the growing protein density (Fig. 4G), accompanied by an increase in the helical pitch from ~15 to ~30 nm (Fig. 4E), and a net complex elongation of ~1.5-fold (Fig. S2A) with respect to a ~1000-fold increase in bulk protein concentration. The observed variation in helical structure is based on concentration-dependent shifts in the protein-DNA contour length, associated with filament unwinding. These data were extracted from fits to DNA stretching curves up to 5 pN (Fig. 4A, C) in order to reduce the effect of tension on the structure of the protein-DNA filament. Moreover, increased complex elongation (i.e., transition to a less wound conformation) was significant down to ~1 pN tension (Fig. 4A inset), and the force-extension curves were well fit by the worm-like chain in this region. This suggests that unwinding of the gp32-ssDNA complex is not merely a high force phenomenon (Fig. 3) but that critical filament rearrangements also occur at low forces (≤ 5 pN), typical of intracellular processes [53]. This impressive ability of the gp32-ssDNA complex to adjust its helical structure to the bulk solution conditions may reflect the necessity of the ssDNA to be gp32-protected from degradation (e.g., nuclease attack) in the wide range of protein levels in the nucleus.

The helical protein-DNA filament remains highly cooperative and stable in a broad range of protein concentrations, as reported by slow (linear) gp32 dissociation from the few filament ends (Fig. 5). However, at very high levels of ssDNA saturation, leading to a reduction in the protein binding site size to ~6 nt, the WT gp32 filament becomes unstable, as observed by the appearance of a rapid exponential dissociation phase not seen at lower complex saturation. For WT gp32, this occurs at bulk protein concentrations ≥ 300 nM (in 50 mM Na^+), resulting in a reduction in the twist angle between neighboring proteins to ~50° [14]. At these high WT gp32 concentrations, untwisting of the filament upon additional protein binding becomes energetically unfavorable, leading to weakening of the protein-protein contacts and a loss of binding cooperativity. Bringing such complexes into protein-free solution results in prompt, noncooperative dissociation from across the entire ssDNA template on a ~10 s timescale (Fig. 5B), comparable to the rate of ssDNA dissociation from the noncooperative gp32 variants, *II and *III (Fig. 2). Fast, exponential gp32 dissociation continues until enough protein is released from the filament to return the gp32-ssDNA complex to its stable, moderately unwound state. At this point, the filament becomes highly cooperative again, and protein dissociation occurs over a much longer timescale only from the filament ends (Fig. 6D). In our previous work [14], we hypothesized that this fast, noncooperative gp32 dissociation from its oversaturated complex with ssDNA can provide a mechanism for rapid protein removal from the template that can keep pace with DNA synthesis by the fast moving [54] polymerase (Fig. 7). This local gp32-ssDNA complex overcrowding could be produced by rapid polymerase movement itself, thereby providing a plausible mechanism for autoregulation of the rate of gp32 filament dissociation during DNA replication.

The main finding of the present work is our demonstration that, relative to WT gp32, the CTD-deletion variant, *I, can bind and unwind the ssDNA helical filament to a much greater extent without inducing filament destabilization. This heavily oversaturated (and unwound) complex remains cooperative and

stable, as reported by saturation level-independent slow protein dissociation from the filament ends only, similar to the dissociation of WT gp32 at much lower saturation levels (Fig. 5C). We hypothesize that the presence of the CTD in the full-length protein leads to limitations in gp32-ssDNA filament unwinding, which manifest under conditions of high protein density (i.e., overcrowding). Indeed, a decrease in the stacking angle (untwisting) between adjacently-bound gp32 proteins should lead to a reduction in the distance between the C-terminal domains at the periphery of the protein helix. This, in turn, could induce either steric or electrostatic repulsion between the neighboring CTDs, leading to destabilization of the protein-protein interactions, facilitating rapid gp32 dissociation that increases exponentially with the level of complex oversaturation (Fig. 5C). Alternatively, a critical change in the relative twist angle between adjacently-bound proteins could place the CTD in an orientation such that it sterically blocks (or interferes with) and directly disrupts the (presumably) CTD-adjacent [23] NTD-core interaction required for protein cooperativity, resulting in gp32-gp32 destabilization across the entire filament.

Irrespective of the detailed nature of this destabilizing CTD clash, it appears to be eliminated upon CTD removal in the *I gp32 variant, leading to a significantly more stable oversaturated ssDNA complex. This result offers a new interpretation of the role of the CTD in mediating prompt displacement of gp32 from the ssDNA template during T4 DNA replication. We propose that the CTD-constrained internal dynamics of the gp32-ssDNA filament (alone) can promote rapid removal of gp32 during genomic processing events, even in the absence of heterotypic protein interactions that are generally thought to be required for efficient turnover (Fig. 7). On the other hand, it is entirely possible that this mode of destabilization is also coupled to direct interactions with the replisomal proteins (e.g., polymerase, helicase, etc.) via the acidic CTD to coordinate yet faster gp32 displacement. However, how these interactions could facilitate stronger gp32 destabilization remains unclear.

During T4 DNA replication, the length of a typical Okazaki fragment is 1000-2000 nt [55]. Our proposed mechanism of stimulated gp32 displacement through overcrowding on ssDNA becomes more efficient on these longer templates. This is because such destabilized filaments are noncooperative, resulting in exponential dissociation from across the entire DNA segment, and the number of proteins dissociating per unit time is proportional to the filament length. As a ~2000 nt Okazaki fragment binds ~300 gp32 at saturation, our highest measured exponential WT recompaction rate of ~0.1 s^{-1} (Fig. S3B) implies that ~30 proteins dissociate from the oversaturated filament per second. Assuming that in its maximally unwound and elongated conformation each protein occupies ~6 nt of ssDNA (Fig. 4G), we estimate a nucleotide release rate of ~200 nt/s, in good agreement with *in vitro* DNA synthesis rates (~250 nt/s) [54]. Note, the calculated release rate is based on protein dissociation measurements taken at 15 pN tension, a force not often associated with typical intracellular mechanisms. However, previous single molecule DNA stretching experiments have shown that polymerases can generate forces on ssNA templates as high as ~15 to 35 pN during synthesis of the complementary strand [56-60], suggesting that the behavior observed here is likely to be applicable to DNA replication processes *in vivo*. Thus, prompt gp32 displacement via filament restructuring may be able to keep pace with the rapidly moving replication fork without requiring the assistance of other replication proteins.

In contrast to WT gp32, dissociation of *I occurs primarily from the ends of the cooperative filaments, resulting in much slower linear recompaction that is independent of the length of the substrate. Assuming the length of ssDNA per protein along the helical axis, $h \approx 3$ nm [14], remains constant, we estimate that release of a single *I molecule (followed by filament rewinding) reduces the extension of

the complex by ~3 nm. Assuming prompt re-equilibration of ssDNA rewinding on the remaining filament, our highest measured *I recompaction rate $v = 1 \times 10^{-4}$ nm $nt^{-1}s^{-1} \cdot 8.1$ knt ≈ 1 nm/s (Fig. 6E, S3A) implies that on average, one protein dissociates from the unwound filament every three seconds. Given a binding site size of ~6 nt in the unwound conformation, dissociation of *I from the filament ends yields a nucleotide release rate of ~2 nt/s. Alternatively, we can estimate the rate of ssDNA release from our recompaction curves directly. Transition of the maximally unwound *I-ssDNA filament to its optimally wound state results in an ssDNA extension reduction of $\Delta x \approx 0.05$ nm/nt. Thus, the fastest measured *I recompaction rate (1×10^{-4} nm $nt^{-1}s^{-1}$) yields a dissociation timescale, $\tau \approx 500$ s. Relative to its optimally wound (~7 nt per protein) state, our protein density measurements indicated a ~1.25-fold increase of bound protein in the unwound complex (Fig. 4G), implying that ~300 excess proteins must dissociate from the substrate during this transition. A binding site size of ~6 nt suggests that ~2000 nt of ssDNA are released during this process, yielding a nucleotide release rate of ~4 nt/s, in reasonable agreement with our original estimate. Thus, ssDNA release from the overcrowded template is enhanced significantly (~50 to 100-fold) in the presence of the C-terminal domain, indicating its overall importance in ensuring rapid template clearing during DNA synthesis (Fig. 7). Furthermore, removal of the CTD also increases the dsDNA helix-destabilizing activity of the protein, suggesting that *I might have the ability to bring about the melting of the dsDNA region adjacent to the Okazaki fragment, potentially leading to destabilization and premature dissociation of T4 polymerase [47]. Thus, the absence of the CTD from gp32 likely has multiple deleterious consequences for its role in DNA replication, recombination, and repair.

2.6.2 Presynaptic filament formation

In addition to addressing the role of the gp32 CTD in mediating ssDNA template clearing during DNA synthesis, our proposed model may be applicable to other genomic processes, such as formation of the presynaptic filament, a crucial early step in genetic recombination. With respect to T4 bacteriophage, this reaction involves at least three T4-coded proteins: the recombinase (UvsX), the recombination mediator (UvsY), and gp32. In its final state, the presynaptic filament is composed of UvsX polymerized along the ssDNA. However, intermediate complexes involving both UvsY and gp32 are required for proper loading of the UvsX recombinase. In this regard, UvsY functions as an accessory factor to facilitate displacement of gp32 by UvsX [61, 62].

Early studies on presynaptic filament assembly concluded that direct interactions between UvsY and the gp32 CTD are required for loading of UvsY onto the gp32-saturated ssDNA, and that efficient binding of UvsY is necessary for prompt gp32 removal and subsequent polymerization of UvsX along the DNA [63]. These findings were based on correlated measurements of gp32-UvsY binding (via direct crosslinking) and UvsX polymerization (inferred through rates of ATP hydrolysis), both of which were reduced in the absence of the acidic CTD. However, more recent studies indicated that UvsY and gp32 co-occupy the ssDNA in a noncompetitive fashion, and that heterotypic protein interactions between gp32 and UvsY: (i) are not required for filament formation and (ii) do not affect the affinity of UvsY for the ssDNA substrate [64, 65]. These studies suggested that UvsY destabilizes gp32 binding and remodels the gp32-ssDNA complex through UvsY-ssDNA interactions rather than direct gp32-UvsY interactions.

To explain how the C-terminal domain facilitates gp32 displacement from the presynaptic filament without direct interactions between UvsY or UvsX, we propose a dissociation scheme wherein the binding of additional protein (e.g., UvsY) to the gp32-coated ssDNA molecule induces substrate overcrowding, similar to that observed at high concentrations of free gp32, thereby stimulating CTD-

mediated gp32 destabilization via internal rearrangement of its helical structure (i.e., critical filament unwinding). This model provides a simple, plausible mechanism for gp32 removal that could potentially be the primary mode of rapid ssDNA clearing during T4 DNA replication and recombination, demonstrating its utility in understanding the dynamics of gp32 filament reorganization.

3. Materials and Methods

3.1. Purification of gp32

Full-length gp32 and its truncated forms (*I, *II, and *III) were prepared as previously described [11, 24]. Protein concentrations were determined spectrophotometrically using $\varepsilon_{280}^{M} = 3.7 \times 10^4\ M^{-1}cm^{-1}$ [66].

3.2. Optical tweezers system for measuring ssDNA conformation at constant force

An 8.1 knt ssDNA molecule, tethered between two 1.76 µm diameter streptavidin-coated microbeads, was generated *in situ* as described previously [67] and held at fixed tension. Extension of the ssDNA was continuously adjusted to maintain the given force applied by the trapping laser. Unless otherwise stated, experiments were performed in a binding buffer containing 50 mM Na^+ (45 mM NaCl and 5 mM NaOH) and 10 mM HEPES at pH 7.5. The extension of the ssDNA was controlled by a piezoelectric translational stage with 1 nm precision, and the tension along the substrate was measured by the laser deflection of the stationary optical trap. Constant force experiments were performed at 15 pN tension in order to maximize the ssDNA extension reduction (shortening) during gp32 binding while minimizing the force along the DNA molecule. This tension is sufficient to ensure that the formation of ssDNA secondary structures due to sequence heterogeneity is negligible across all salt conditions used. The distance between the beads was measured using simultaneously recorded bright-field images to calculate the absolute extension of the ssDNA and correct for long-term thermal drift in the system. Following incubation, free protein was removed by exchanging with protein-free buffer. Data were analyzed using custom scripts in MATLAB (MathWorks). All experiments were performed in replicate (N ≥ 3) with uncertainty calculated as standard error of the mean (SEM).

3.3. ssDNA stretching and polymer length measurements

In the presence of various, fixed gp32 concentrations, the ssDNA was slowly stretched at a rate of ~10 nm/s to ensure equilibration at every force. The force-extension curves (FECs) of ssDNA saturated with the noncooperative *II (gp32 lacking its N-terminal domain) and *III (gp32 lacking both its N-terminal and C-terminal domains) truncates were fit with the freely jointed chain (FJC) polymer model [36]

$$x(F) = L\left(\coth\left(\frac{2pF}{k_BT}\right) - \frac{k_BT}{2pF}\right)\left(1 + \frac{F}{S}\right) \tag{2}$$

up to 10 pN to compute the contour and persistence lengths of the complexes, where L is the protein-DNA contour length (end-to-end distance), p is the persistence length, and S is the elastic modulus. FECs of the full-length and *I (gp32 lacking its C-terminal domain) gp32 complexes were fit with the worm-like chain (WLC) model [38, 39]

$$x(F) = L\left(1 - \frac{1}{2}\left(\frac{k_B T}{Fp}\right)^{1/2} + \frac{F}{S}\right) \quad (3)$$

up to 5 pN to compute the contour and persistence lengths as functions of free protein concentration. Uncertainty was calculated as the SEM for best fit parameters derived from three or more replicate curves.

Author Contributions

BAC: Conceptualization, Methodology, Formal analysis, Investigation, Writing- Original draft, Visualization; MM: Methodology, Resources, Writing- Review and editing; IR: Methodology, Writing- Review and editing; RLK: Conceptualization, Resources, Writing- Review and editing, Funding acquisition; MCW: Conceptualization, Resources, Writing- Review and editing, Supervision, Funding acquisition.

Acknowledgements

Funding for this project was provided by the National Science Foundation (MCB-1817712 to MCW), National Institutes of Health (GM 52049 to RLK), and UMBC Designated Research Initiative Fund (to RLK).

Declarations of interest: none

References

[1] Nossal N. Molecular Biology of Bacteriophage T4. Am Soc Microbiol. 1994:43-53.
[2] Alberts BM. Prokaryotic DNA replication mechanisms. Philos Trans R Soc Lond B Biol Sci. 1987;317:395-420.
[3] Johnson A, O'Donnell M. Cellular DNA replicases: components and dynamics at the replication fork. Annu Rev Biochem. 2005;74:283-315.
[4] Mueser TC, Hinerman JM, Devos JM, Boyer RA, Williams KJ. Structural analysis of bacteriophage T4 DNA replication: a review in the Virology Journal series on bacteriophage T4 and its relatives. Virol J. 2010;7:1-16.
[5] Benkovic SJ, Valentine AM, Salinas F. Replisome-mediated DNA replication. Annual review of biochemistry. 2001;70:181-208.
[6] Alberts BM, Frey L. T4 bacteriophage gene 32: a structural protein in the replication and recombination of DNA. Nature. 1970;227:1313-8.
[7] Shamoo Y, Friedman AM, Parsons MR, Konigsberg WH, Steitz TA. Crystal structure of a replication fork single-stranded DNA binding protein (T4 gp32) complexed to DNA. Nature. 1995;376:362-6.
[8] Theobald DL, Mitton-Fry RM, Wuttke DS. Nucleic acid recognition by OB-fold proteins. Annu Rev Biophys Biomol Struct. 2003;32:115-33.
[9] Huang C, Hearst J, Alberts B. Two types of replication proteins increase the rate at which T4 DNA polymerase traverses the helical regions in a single-stranded DNA template. J Biol Chem. 1981;256:4087-94.
[10] Karpel RL. T4 bacteriophage gene 32 protein. The biology of nonspecific DNA protein interactions CRC Press, Inc, Boca Raton, Fla. 1990:103-30.
[11] Wu M, Flynn EK, Karpel RL. Details of the nucleic acid binding site of T4 gene 32 protein revealed by proteolysis and DNA Tm depression methods. J Mol Biol. 1999;286:1107-21.

[12] Casas-Finet JR, Fischer KR, Karpel RL. Structural basis for the nucleic acid binding cooperativity of bacteriophage T4 gene 32 protein: the (Lys/Arg)3(Ser/Thr)2 (LAST) motif. Proc Natl Acad Sci U S A. 1992;89:1050-4.
[13] Lonberg N, Kowalczykowski SC, Paul LS, von Hippel PH. Interactions of bacteriophage T4-coded gene 32 protein with nucleic acids. III. Binding properties of two specific proteolytic digestion products of the protein (G32P*I and G32P*III). J Mol Biol. 1981;145:123-38.
[14] Cashen BA, Morse M, Rouzina I, Karpel RL, Williams MC. Dynamic structure of T4 gene 32 protein filaments facilitates rapid noncooperative protein dissociation. Nucleic Acids Res. 2023;51:8587-605.
[15] Kuil ME, van der Oord CJ, Vlaanderen CA, van Haeringen B, van Grondelle R. A refined calculation of the solution dimensions of the complex between gene 32 protein and single stranded DNA based on estimates of the bending persistence length. J Biomol Struct Dyn. 1990;7:943-57.
[16] Scheerhagen MA, Kuil ME, van Amerongen H, van Grondelle R. A model for the complex between the helix destabilizing protein GP32 of bacteriophage T4 and single-stranded DNA. J Biomol Struct Dyn. 1989;6:701-6.
[17] Scheerhagen MA, Kuil ME, van Grondelle R, Blok J. Hydrodynamic studies of a DNA-protein complex. Dimensions of the complex of single-stranded 145 base DNA with gene 32 protein of phage T4 deduced from quasi-elastic light scattering. FEBS Lett. 1985;184:221-5.
[18] Scheerhagen MA, van Amerongen H, van Grondelle R, Blok J. Hydrodynamic studies of a DNA-protein complex. Elongation of single stranded nucleic acids upon complexation with the gene 32 protein of phage T4 deduced from electric field-induced birefringence experiments. FEBS Lett. 1985;179:221-4.
[19] van Amerongen H, Kuil ME, Scheerhagen MA, van Grondelle R. Structure calculations for single-stranded DNA complexed with the single-stranded DNA binding protein GP32 of bacteriophage T4: a remarkable DNA structure. Biochemistry. 1990;29:5619-25.
[20] Lohman TM. Kinetics and mechanism of dissociation of cooperatively bound T4 gene 32 protein-single-stranded nucleic acid complexes. 1. Irreversible dissociation induced by sodium chloride concentration jumps. Biochemistry. 1984;23:4656-65.
[21] Lohman TM. Kinetics and mechanism of dissociation of cooperatively bound T4 gene 32 protein-single-stranded nucleic acid complexes. 2. Changes in mechanism as a function of sodium chloride concentration and other solution variables. Biochemistry. 1984;23:4665-75.
[22] Rouzina I, Pant K, Karpel RL, Williams MC. Theory of electrostatically regulated binding of T4 gene 32 protein to single- and double-stranded DNA. Biophys J. 2005;89:1941-56.
[23] Karpel RL. LAST motifs and SMART domains in gene 32 protein: an unfolding story of autoregulation? IUBMB Life. 2002;53:161-6.
[24] Waidner LA, Flynn EK, Wu M, Li X, Karpel RL. Domain effects on the DNA-interactive properties of bacteriophage T4 gene 32 protein. J Biol Chem. 2001;276:2509-16.
[25] Pant K, Karpel RL, Rouzina I, Williams MC. Mechanical measurement of single-molecule binding rates: kinetics of DNA helix-destabilization by T4 gene 32 protein. J Mol Biol. 2004;336:851-70.
[26] Pant K, Karpel RL, Rouzina I, Williams MC. Salt dependent binding of T4 gene 32 protein to single and double-stranded DNA: single molecule force spectroscopy measurements. J Mol Biol. 2005;349:317-30.
[27] Pant K, Karpel RL, Williams MC. Kinetic regulation of single DNA molecule denaturation by T4 gene 32 protein structural domains. J Mol Biol. 2003;327:571-8.
[28] Hosoda J, Takacs B, Brack C. Denaturation of T4 DNA by an in vitro processed gene 32-protein. FEBS letters. 1974;47:338-42.
[29] Krassa KB, Green LS, Gold L. Protein-protein interactions with the acidic COOH terminus of the single-stranded DNA-binding protein of the bacteriophage T4. Proc Natl Acad Sci U S A. 1991;88:4010-4.

[30] Lefebvre SD, Wong ML, Morrical SW. Simultaneous interactions of bacteriophage T4 DNA replication proteins gp59 and gp32 with single-stranded (ss) DNA. Co-modulation of ssDNA binding activities in a DNA helicase assembly intermediate. J Biol Chem. 1999;274:22830-8.
[31] Morrical SW, Beernink HT, Dash A, Hempstead K. The gene 59 protein of bacteriophage T4. Characterization of protein-protein interactions with gene 32 protein, the T4 single-stranded DNA binding protein. J Biol Chem. 1996;271:20198-207.
[32] Nelson SW, Kumar R, Benkovic SJ. RNA primer handoff in bacteriophage T4 DNA replication: the role of single-stranded DNA-binding protein and polymerase accessory proteins. J Biol Chem. 2008;283:22838-46.
[33] Hurley JM, Chervitz SA, Jarvis TC, Singer BS, Gold L. Assembly of the bacteriophage T4 replication machine requires the acidic carboxy terminus of gene 32 protein. J Mol Biol. 1993;229:398-418.
[34] Perumal SK. A real-time fluorescent gp32 probe-based assay for monitoring single-stranded DNA-dependent DNA processing enzymes. Biochem Biophys Rep. 2023;35:101518.
[35] Pant K, Anderson B, Perdana H, Malinowski MA, Win AT, Pabst C, et al. The role of the C-domain of bacteriophage T4 gene 32 protein in ssDNA binding and dsDNA helix-destabilization: Kinetic, single-molecule, and cross-linking studies. PLoS One. 2018;13:e0194357.
[36] Smith SB, Cui Y, Bustamante C. Overstretching B-DNA: the elastic response of individual double-stranded and single-stranded DNA molecules. Science. 1996;271:795-9.
[37] Lohman TM, Kowalczykowski SC. Kinetics and mechanism of the association of the bacteriophage T4 gene 32 (helix destabilizing) protein with single-stranded nucleic acids. Evidence for protein translocation. J Mol Biol. 1981;152:67-109.
[38] Baumann CG, Smith SB, Bloomfield VA, Bustamante C. Ionic effects on the elasticity of single DNA molecules. Proc Natl Acad Sci U S A. 1997;94:6185-90.
[39] Odijk T. Stiff Chains and Filaments under Tension. Macromolecules. 1995;28:7016-8.
[40] Kuil ME, van Mourik F, Burger W, van Grondelle R. The internal dynamics of gene 32 protein-DNA complexes studied by quasi-elastic light scattering. Biophys Chem. 1988;32:211-27.
[41] van der Heijden T, Dekker C. Monte carlo simulations of protein assembly, disassembly, and linear motion on DNA. Biophys J. 2008;95:4560-9.
[42] Cheng X, Guinn EJ, Buechel E, Wong R, Sengupta R, Shkel IA, et al. Basis of Protein Stabilization by K Glutamate: Unfavorable Interactions with Carbon, Oxygen Groups. Biophys J. 2016;111:1854-65.
[43] Richey B, Cayley D, Mossing M, Kolka C, Anderson CF, Farrar TC, et al. Variability of the intracellular ionic environment of Escherichia coli. Differences between in vitro and in vivo effects of ion concentrations on protein-DNA interactions and gene expression. J Biol Chem. 1987;262:7157-64.
[44] Kozlov AG, Cheng X, Zhang H, Shinn MK, Weiland E, Nguyen B, et al. How Glutamate Promotes Liquid-liquid Phase Separation and DNA Binding Cooperativity of E. coli SSB Protein. J Mol Biol. 2022;434:167562.
[45] Kozlov AG, Shinn MK, Weiland EA, Lohman TM. Glutamate promotes SSB protein-protein Interactions via intrinsically disordered regions. J Mol Biol. 2017;429:2790-801.
[46] Kowalczykowski SC, Lonberg N, Newport JW, von Hippel PH. Interactions of bacteriophage T4-coded gene 32 protein with nucleic acids. I. Characterization of the binding interactions. J Mol Biol. 1981;145:75-104.
[47] Burke RL, Alberts BM, Hosoda J. Proteolytic removal of the COOH terminus of the T4 gene 32 helix-destabilizing protein alters the T4 in vitro replication complex. J Biol Chem. 1980;255:11484-93.
[48] Richardson RW, Nossal NG. Trypsin cleavage in the COOH terminus of the bacteriophage T4 gene 41 DNA helicase alters the primase-helicase activities of the T4 replication complex in vitro. J Biol Chem. 1989;264:4732-9.
[49] Huberman JA, Kornberg A, Alberts BM. Stimulation of T4 bacteriophage DNA polymerase by the protein product of T4 gene 32. J Mol Biol. 1971;62:39-52.

[50] Ishmael FT, Alley SC, Benkovic SJ. Identification and mapping of protein-protein interactions between gp32 and gp59 by cross-linking. J Biol Chem. 2001;276:25236-42.
[51] Jones CE, Mueser TC, Dudas KC, Kreuzer KN, Nossal NG. Bacteriophage T4 gene 41 helicase and gene 59 helicase-loading protein: a versatile couple with roles in replication and recombination. Proc Natl Acad Sci U S A. 2001;98:8312-8.
[52] Trakselis MA, Roccasecca RM, Yang J, Valentine AM, Benkovic SJ. Dissociative properties of the proteins within the bacteriophage T4 replisome. J Biol Chem. 2003;278:49839-49.
[53] Yusko EC, Asbury CL. Force is a signal that cells cannot ignore. Mol Biol Cell. 2014;25:3717-25.
[54] Mace DC, Alberts BM. T4 DNA polymerase. Rates and processivity on single-stranded DNA templates. J Mol Biol. 1984;177:295-311.
[55] Maloy S, Hughes K. Brenner's encyclopedia of genetics: Academic Press; 2013.
[56] Bustamante C, Bryant Z, Smith SB. Ten years of tension: single-molecule DNA mechanics. Nature. 2003;421:423-7.
[57] John R, Davenport n, Wuite GJ, Landick R, Bustamante C. Single-molecule study of transcriptional pausing and arrest by E. coli RNA polymerase. Science. 2000;287:2497-500.
[58] Wang MD, Schnitzer MJ, Yin H, Landick R, Gelles J, Block SM. Force and velocity measured for single molecules of RNA polymerase. Science. 1998;282:902-7.
[59] Wuite GJ, Smith SB, Young M, Keller D, Bustamante C. Single-molecule studies of the effect of template tension on T7 DNA polymerase activity. Nature. 2000;404:103-6.
[60] Yin H, Wang MD, Svoboda K, Landick R, Block SM, Gelles J. Transcription against an applied force. Science. 1995;270:1653-7.
[61] Bleuit JS, Xu H, Ma Y, Wang T, Liu J, Morrical SW. Mediator proteins orchestrate enzyme-ssDNA assembly during T4 recombination-dependent DNA replication and repair. Proc Natl Acad Sci U S A. 2001;98:8298-305.
[62] Pant K, Shokri L, Karpel RL, Morrical SW, Williams MC. Modulation of T4 gene 32 protein DNA binding activity by the recombination mediator protein UvsY. J Mol Biol. 2008;380:799-811.
[63] Jiang H, Giedroc D, Kodadek T. The role of protein-protein interactions in the assembly of the presynaptic filament for T4 homologous recombination. J Biol Chem. 1993;268:7904-11.
[64] Liu J, Qian N, Morrical SW. Dynamics of bacteriophage T4 presynaptic filament assembly from extrinsic fluorescence measurements of Gp32-single-stranded DNA interactions. J Biol Chem. 2006;281:26308-19.
[65] Sweezy MA, Morrical SW. Biochemical interactions within a ternary complex of the bacteriophage T4 recombination proteins uvsY and gp32 bound to single-stranded DNA. Biochemistry. 1999;38:936-44.
[66] Jensen DE, Kelly R, von Hippel PH. DNA" melting" proteins. II. Effects of bacteriophage T4 gene 32-protein binding on the conformation and stability of nucleic acid structures. J Biol Chem. 1976;251:7215-28.
[67] Morse M, Sefcikova J, Rouzina I, Beuning PJ, Williams MC. Structural domains of SARS-CoV-2 nucleocapsid protein coordinate to compact long nucleic acid substrates. Nucleic Acids Res. 2023;51:290-303.

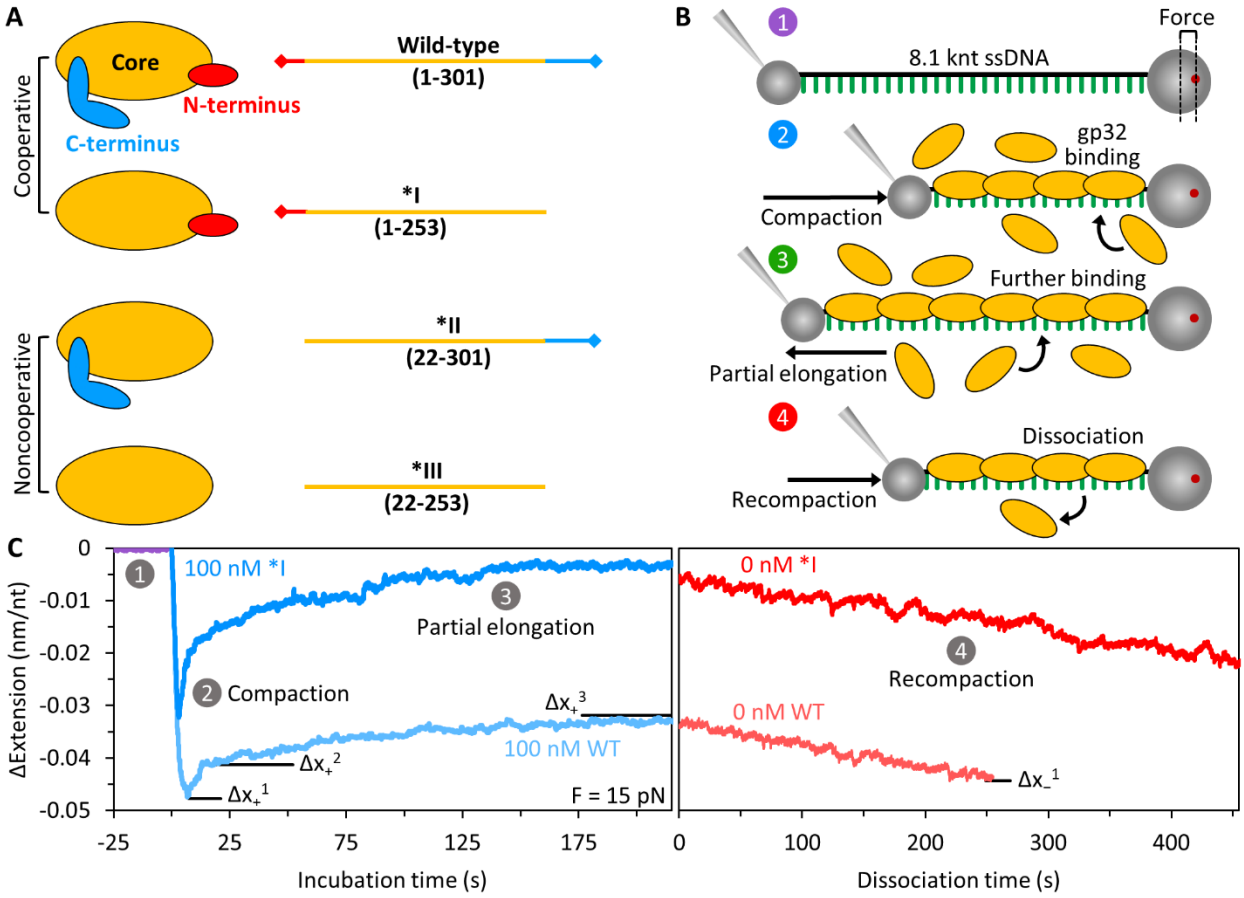

Figure 1: Measuring gp32 binding and ssDNA conformation. (A) Wild-type (WT) gp32 comprises three domains: the N-terminal domain (NTD, red), ssDNA binding core (yellow), and the C-terminal domain (CTD, blue). In addition to full-length (301 aa) gp32, three truncates, missing the CTD (*I), NTD (*II), or both (*III), were used. (B) An 8.1 knt ssDNA molecule was tethered between two functionalized microbeads and held at a fixed tension as measured by beam deflection in the optical trap (1). The DNA extension was continuously adjusted to maintain constant tension during incubation with free protein (2, 3) and its subsequent removal (4) to measure gp32 binding and dissociation. (C) In the presence of 100 nM WT gp32 (light blue), the DNA exhibits multiphasic length changes consistent with its winding (2) and unwinding (3) by the cooperative protein filaments: an initial fast compaction (Δx_+^1) followed by two distinct elongation events with different kinetic rates ($\Delta x_+^1 \rightarrow \Delta x_+^2$ and $\Delta x_+^2 \rightarrow \Delta x_+^3$). Incubation with 100 nM *I (blue) results in a similar, albeit significantly less compact, binding profile. Upon removal of free protein, initial dissociation results in linear substrate recompaction (Δx_-^1) for both the WT gp32 (light red) and *I (red) complexes.

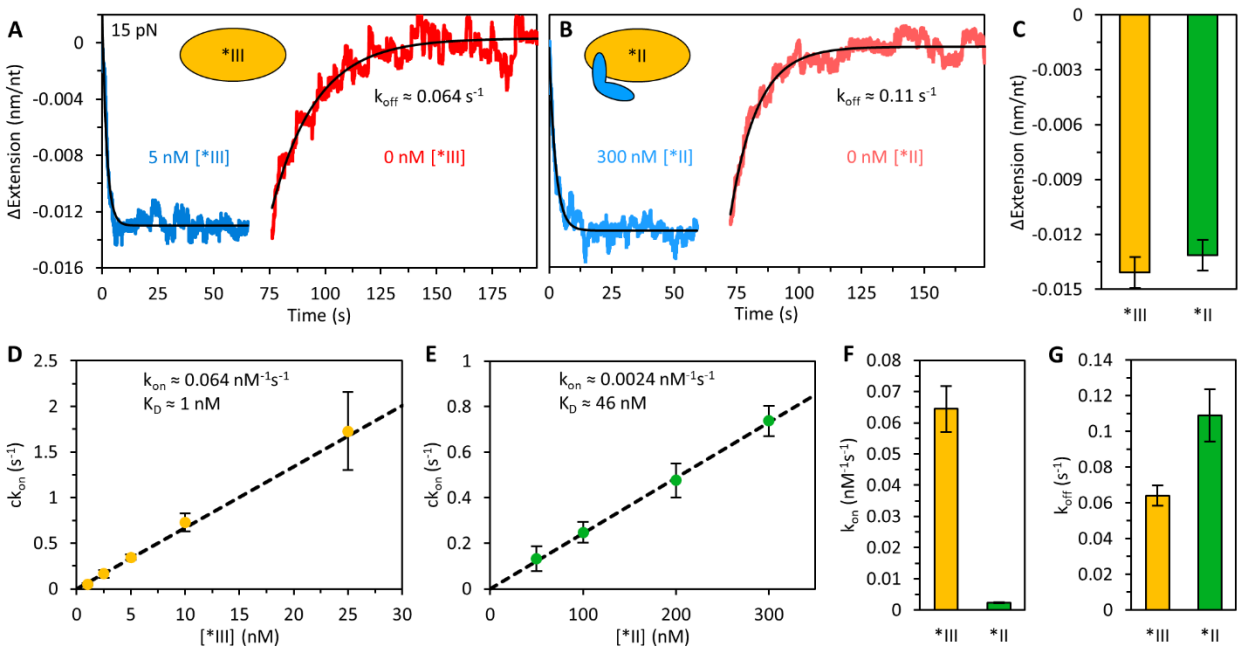

Figure 2: Binding dynamics of noncooperative NTD truncates. The *III (A, without CTD) and *II (B, with CTD) gp32 truncates exhibit single-phased binding (blue) with significantly reduced compaction relative to their cooperative counterparts. When free protein is removed (red), the ssDNA exponentially elongates back to its original length on a ~10 s timescale, consistent with full dissociation of protein. (C) The average equilibrium compaction of the ssDNA at saturation is approximately equivalent for both proteins. (D) The measured rates of protein binding (ck_{on}) are directly proportional to protein concentration and linearly fit to compute the concentration-independent bimolecular on-rate and K_D of *III (D) and *II (E) at 15 pN. (F) The bimolecular binding rate (k_{on}) of *III is ~25-fold higher than *II. (G) The *III off-rate (k_{off}) is ~2-fold lower than that of *II.

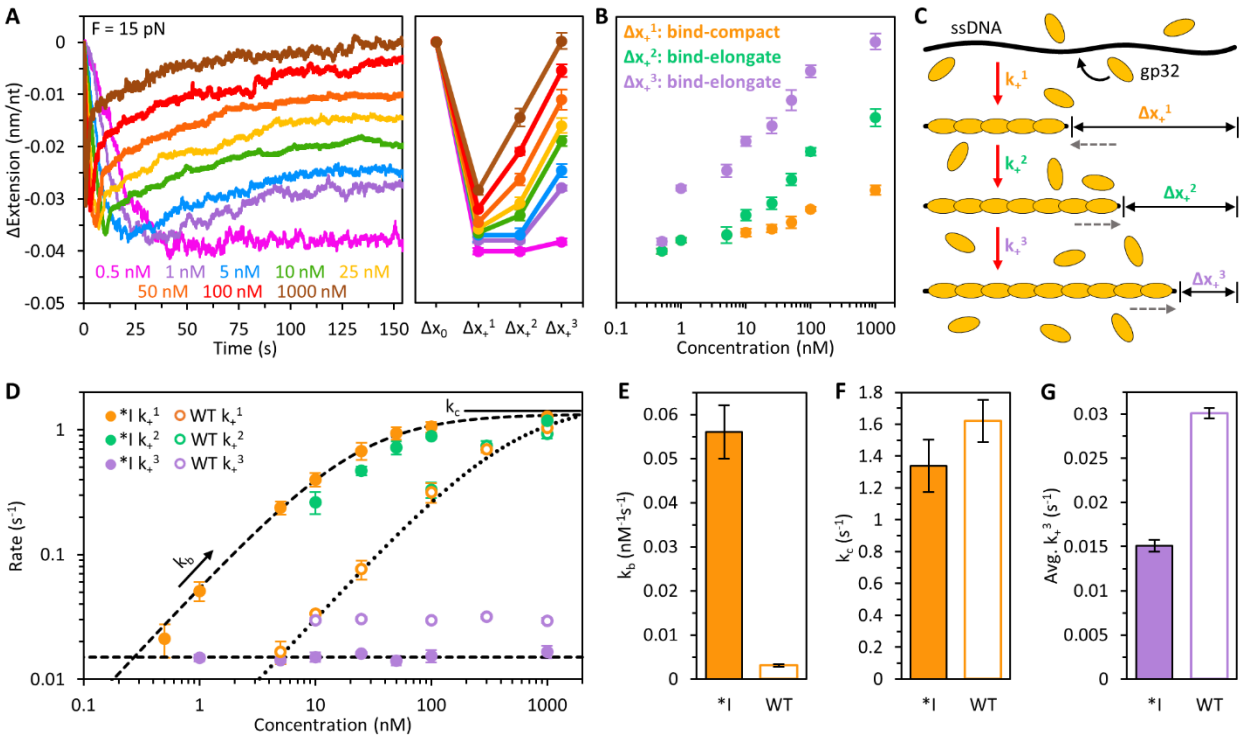

Figure 3: Concentration dependence of *I binding. (A) Representative curves (left) and average extension changes (right) associated with the binding of *I as a function of free protein concentration at 15 pN. Both the maximum initial (Δx_+^1) and equilibrium (Δx_+^3) compaction of the ssDNA decrease with protein concentration. Rapid elongation ($\Delta x_+^1 \rightarrow \Delta x_+^2$) subsequent to initial compaction, but prior to slow elongation, is only observed at [*I] ≥ 10 nM. The slow, secondary elongation step ($\Delta x_+^2 \rightarrow \Delta x_+^3$) is absent at [*I] < 1 nM as the protein-DNA complex equilibrates to a highly compact state. Under conditions in which we observe biphasic elongation, the curves are fit with a two-rate decaying exponential to extract the rates and amplitudes of those phases. (B) Average extension changes (replotted from panel A) associated with each binding phase are plotted as a function of *I concentration. (C) Cartoon illustrating the distinct steps (compaction, fast elongation, and slow elongation) of ssDNA compaction and elongation observed during *I binding. (D) The rate of each binding phase is calculated as a function of *I concentration (filled circles) and compared with WT gp32 (empty circles). The rate of compaction (k_+^1, orange) initially increases linearly with concentration for both proteins before reaching an asymptote at high concentration (fits for *I and WT gp32 are shown as dashed and dotted lines, respectively). The rate of rapid elongation (k_+^2, green) is slightly slower than the initial compaction rate but exhibits a similar increase with protein concentration. While both proteins exhibit qualitatively comparable concentration-dependent kinetics that asymptote to similar values, the rates associated with *I binding are shifted to lower concentrations relative to WT gp32. The slower, secondary elongation phase of *I (k_+^3, purple) is independent of free protein concentration. (E) The *I on-rate, k_b (defined by the slope of k_+^1 vs [gp32] at low concentration), is ~20-fold higher than that of WT gp32. (F) The rate of subsequent compaction due to initial gp32 oligomerization, k_c (defined by the asymptote of k_+^1 at high concentration), is approximately equivalent for both proteins. (G) The average *I k_+^3 value (calculated by fitting k_+^3 vs [gp32] to a straight line) is ~2-fold lower than that of the full-length protein.

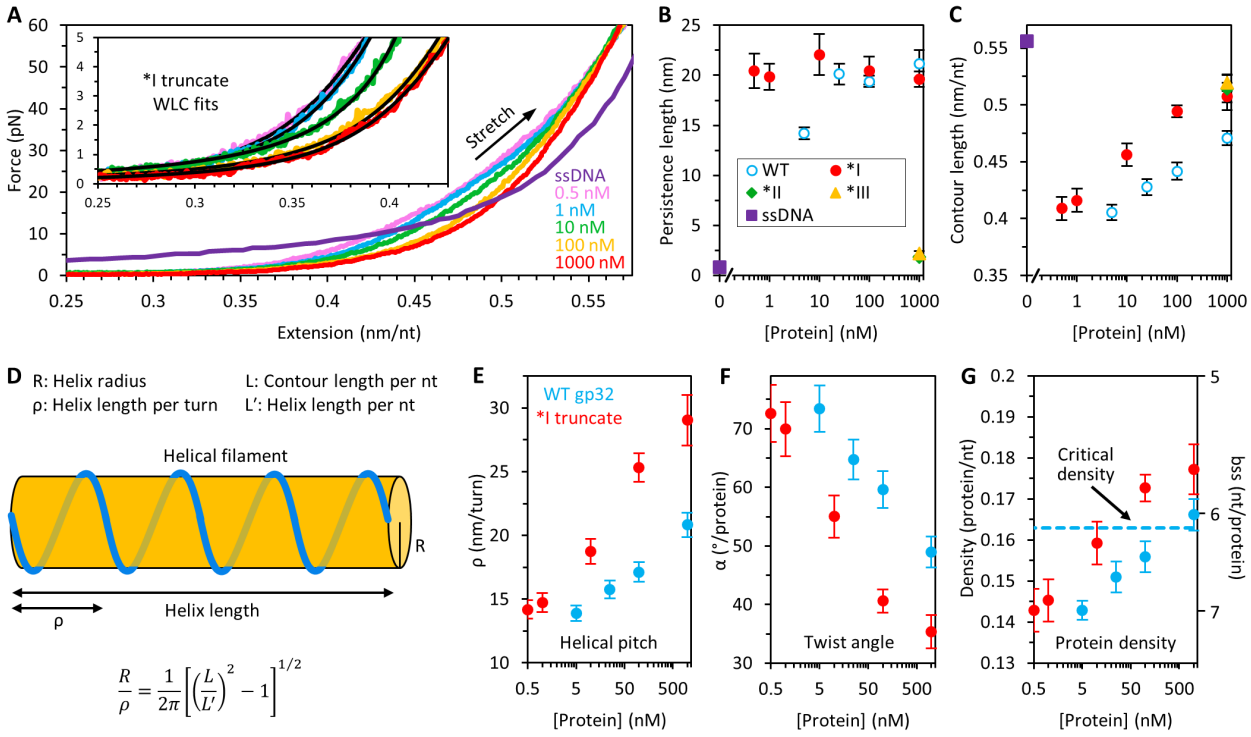

Figure 4: Polymer and helical parameters of gp32-ssDNA complexes. (A) Representative DNA stretching curves in the presence of different concentrations of *I. The gp32-ssDNA complexes are more elongated than bare ssDNA (purple) at low force due to increased persistence length, but shorter (more compact) than ssDNA at high force due to decreased contour length. The force-extension curves are fit with the worm-like chain (WLC, black lines) model up to 5 pN (inset) to compute the contour and persistence lengths of the *I-ssDNA complex, with higher [*I] increasing the extension of the DNA. (B) Persistence lengths of bare ssDNA (purple square) and ssDNA saturated with WT gp32 (blue empty circles), *I (red filled circles), *II (green diamond), and *III (yellow triangle). The WT and *I complexes exhibit significantly greater (longer) persistence lengths than the noncooperative *II and *III gp32 truncates. The persistence length of *I remains constant across the range of concentrations studied and agrees with the persistence length of WT (~20 nm) at high concentration (≥ 25 nM). (C) The contour length reductions (relative to bare ssDNA) of the cooperative gp32 complexes (WT and *I) are greater (more compact) than those of their noncooperative counterparts (*II and *III), but decrease with protein concentration. At similar concentrations, the *I complex exhibits a smaller contour length reduction (less compact) than WT gp32. (D) Geometrical model of an ideal protein-DNA helix relating the ssDNA contour length (*L*), helix length (length along translational axis, *L'*), radius (*R*) and pitch (*ρ*). The *I-ssDNA helix parameters (red) are calculated as functions of protein concentration and compared with those previously calculated for WT gp32 (blue). (E) Under similar concentrations, the *I helical pitch (*ρ*) is greater than that of WT, increasing with protein concentration. (F) The twist angle between neighboring *I proteins (*α*) is generally smaller than that of WT and decreases with concentration. (G) The protein density increases while the binding site size (*bss*, secondary axis) decreases with concentration. The protein density at which we begin to observe rapid, exponential WT dissociation (see Fig. 5B) is indicated by a dashed line in panel G.

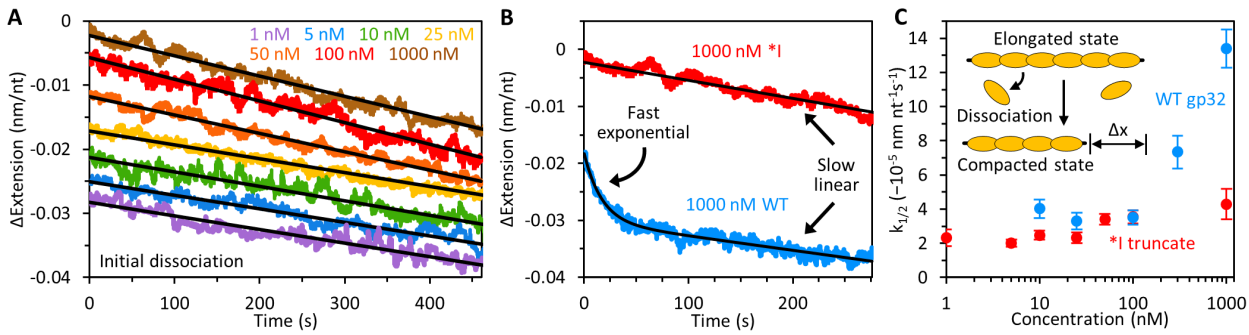

Figure 5: Concentration dependence of *I dissociation. (A) Representative curves showing the initial dissociation phase (recompaction) of *I as a function of incubation concentration. Across all protein concentrations, recompaction of the *I-ssDNA complex is strictly linear in time and fit with a straight line to compute the rate of initial dissociation. (B) At high concentrations (1000 nM), DNA recompaction remains linear for *I, while WT gp32 exhibits two distinct dissociation phases: an initial rapid exponential recompaction followed by a slower linear recompaction step. (C) At concentrations ≤ 100 nM, the estimated rate of recompaction ($k_{1/2}$) is similar for both proteins. However, at higher concentrations, the WT recompaction rate increases significantly, sharply diverging from that of the *I complex.

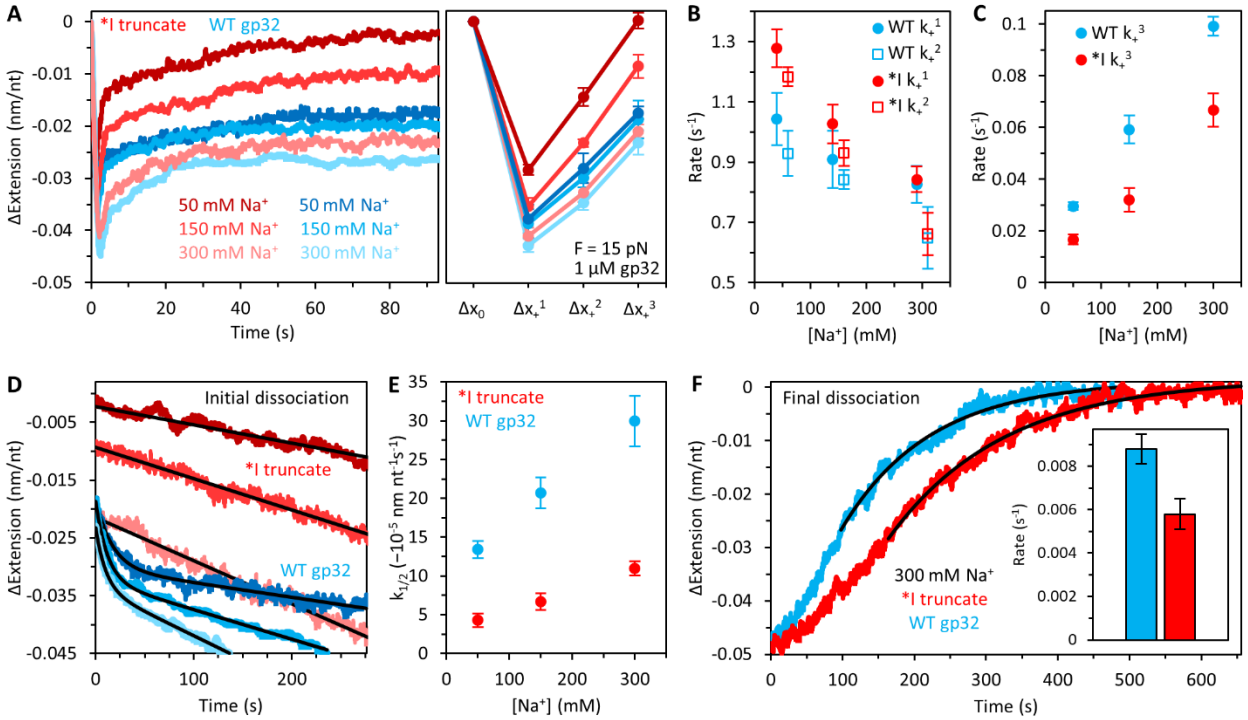

Figure 6: Salt dependence of *I and WT gp32 binding and dissociation. (A) Representative curves (left) and average extension changes (right) associated with the binding of 1 µM *I (red) and WT gp32 (blue) as a function of Na^+ concentration (45, 145, and 295 mM NaCl + 5 mM NaOH) at 15 pN. Both protein complexes exhibit an increase in initial transient compaction (Δx_+^1) and equilibrium compaction (Δx_+^3) with Na^+ concentration. However, the binding profile of *I shows a greater response with salt, converging with that of WT gp32 at high [Na^+]. (B) The rates of both initial compaction (k_+^1, circles) and rapid elongation (k_+^2, squares) decrease with [Na^+]. The kinetics of the corresponding *I (red) and WT (blue) binding phases converge at high salt. Note, data points are offset for clarity. (C) In contrast, the slow, secondary elongation rate (k_+^3) increases with [Na^+] for both proteins but remains moderately slower for the *I complex. (D) Representative curves associated with the initial dissociation phase (recompaction) of *I (red) and WT gp32 (blue) as a function of Na^+ concentration (same as in panel A). The dissociation profile of *I remains linear in time with increased salt, while WT gp32 exhibits biphasic dissociation: an initial exponential recompaction followed by a slower linear recompaction step. The WT gp32 curves are fit with the sum of a linear and single decaying exponential function to extract the rates of both compaction phases (see Fig. S3A-B). (E) The estimated recompaction rate ($k_{1/2}$) increases with [Na^+] for both proteins but remains ~3-fold slower for the *I complex. (F) Representative curves and average rates (inset) associated with the final dissociation phase of *I and WT gp32 at 300 mM Na^+. Under high salt conditions, the final dissociation rate of *I is slightly slower than that of the full-length protein.

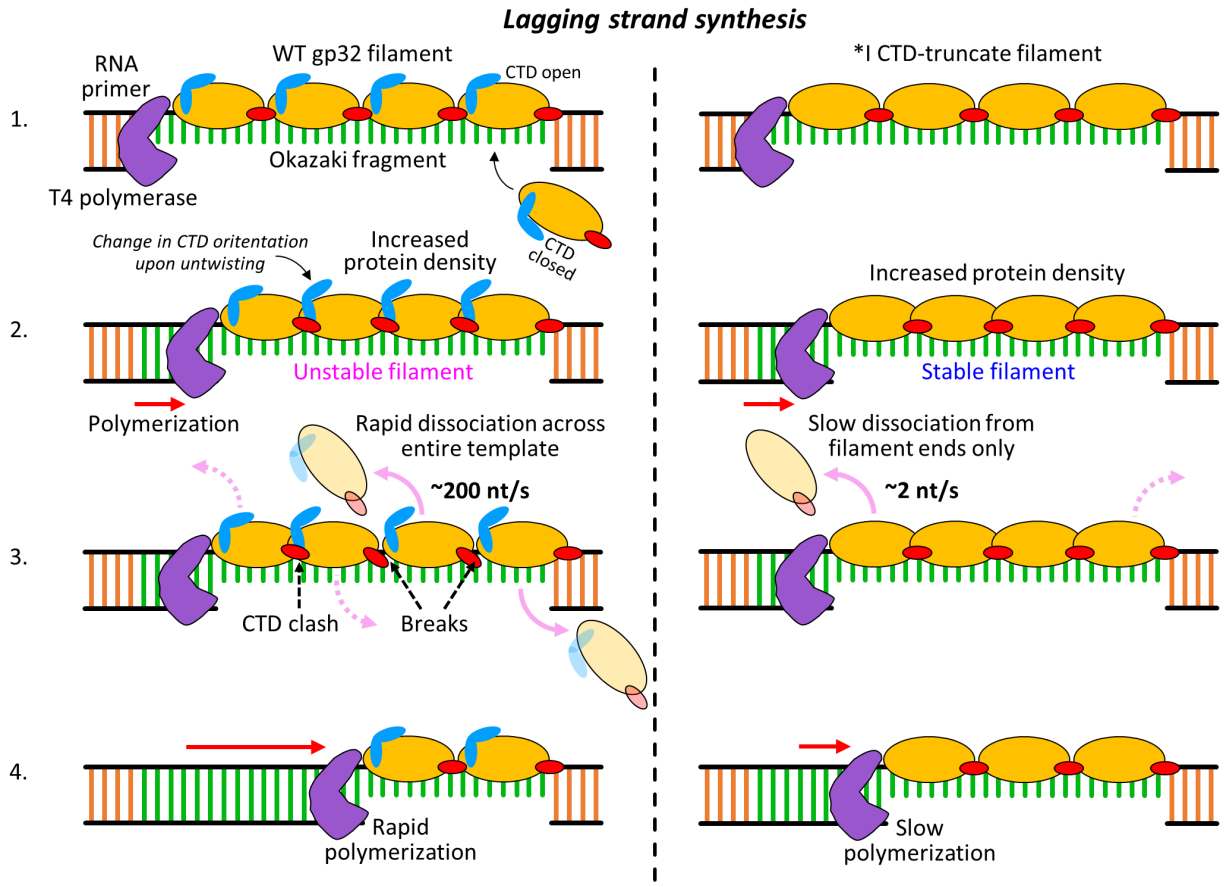

Figure 7: Role of CTD during DNA replication. Diagram illustrating a model for the function of gp32's C-terminal domain in stimulating protein displacement during DNA replication. During lagging strand synthesis, Okazaki fragments are rapidly coated with stable, tightly-bound gp32 filaments (1). This process requires release of the CTD (opening) near the protein's binding site followed by nucleation and protein-protein binding. Polymerization along the DNA template drives an increase in protein density as the ssDNA segment shortens (2). Increased protein density forces the WT gp32 filament (left) into a less stable conformation as the proteins untwist, modulating the orientation of their C-terminal domains. CTD-meditated filament destabilization via protein overcrowding results in fast (~200 nt/s), noncooperative WT dissociation from across the entire ssDNA template (3), thereby clearing the way for rapid strand synthesis (4). This mechanism enables a self-regulating process of protein displacement in which gp32 is readily removed from the template via polymerase-induced overcrowding while also ensuring maximal coverage of the ssDNA at all times. In contrast, upon removal of the CTD, gp32 remains stable and cooperative, regardless of increases in protein density (right), resulting in slow unbinding (~2 nt/s) from the ends of the filament only, inhibiting prompt polymerization.